

Deposition of Nickel-tungsten-phosphorus Coatings on Pure Copper in a Saline Water Environment

Pei-Jing Teng¹, Chien-Hung Lin^{1,*}, Shih-Wei Mao²

¹ Department of Physics, ROC Military Academy, Feng-Shan, Kaohsiung 830, Taiwan

² Department of Mechanical Engineering, ROC Military Academy, Feng-Shan, Kaohsiung 830, Taiwan

*E-mail: linhungcma@gmail.com

Received: 3 September 2020 / Accepted: 4 November 2020 / Published: 31 December 2020

Corrosion of copper caused by chloride species restricts advances in the maritime industry. In the present study, ternary Ni-W-P alloys were electrodeposited on copper in DC current mode to improve the corrosion resistance of the matrix. Then, a SEM equipped with EDAX was employed to investigate the surface morphology and texture of the coating layer. These coatings demonstrated dense microstructures with nodular shapes and few defects in morphology. Potentiostatic polarization and open-circuit tests were employed to investigate the corrosion resistance of the copper matrix with and without coating in 3.5 wt% NaCl. Additionally, a high phosphorus content (ranging from 11-14 wt%) enhanced the corrosion resistance of the coated copper matrix. The corrosion currents (I_{corr}) of the copper without and with coating were 5.72E^{-5} A/cm² and 7.01E^{-7} A/cm², respectively. In the open-circuit test, the corrosive rate decreased when the passive film existed on the surface, while the ternary Ni-W-P coating was exposed to saline water. A slow-strain-rate test (SSRT) was performed in the atmosphere and saline water to evaluate the mechanical properties of the specimens. The strengths of the copper matrix with and without coating were 310 MPa and 240 MPa, respectively. The ternary Ni-W-P coating effectively increased the ultimate tensile strength (UTS) of the substrate during the slow-strain-rate test (SSRT). Furthermore, the specimen seriously deteriorated in the saline water, and it was accompanied by partial brittle fracture due to stress cracking on the adjacent failure surface.

Keywords: ternary Ni-W-P coating, saline water, copper matrix, slow-strain-rate test (SSRT)

1. INTRODUCTION

Copper has been used extensively in the pipeline and electrical industries due to its electrical and thermal conductivity, flexibility and weldability [1]. In marine engineering, principal components of copper demonstrate performance deterioration by dissolved oxygen and chloride species. Cuprous oxide initiates the tendency to uniform corrosion on the cuprite after anodic dissolution. In the literature, nickel-alloy coatings have been employed to inhibit copper corrosion [2-9].

The open circuit potential (OCP) has been measured to evaluate the corrosion resistance of Ni-P and Ni-B coatings in 3.5% NaCl. Initially, the trend of the potential shifted positively with time, while a passive film appeared on the single-coating layer [10]. Then, the potential shifted negatively with the occurrence of a local corrosion coating layer. Moreover, the multilayer coating demonstrated superior performance compared to the single-layer coating during its immersion in saline water for 1500 minutes. The corrosion resistance and mechanical properties of Ni and Ni-W coating layers after an annealing process were discussed by [11]. The interstitial solid inhibited grain growth, and random grains existed on the Ni-W layer after heat treatment. In addition, the finer grain enhanced the toughness of the specimen, and the high-angle grain suppressed the movement of dislocations. The Ni-W coating demonstrated superior resistance to the Ni coating layer when immersed in a 3.5 wt% NaCl solution.

The ternary Ni-W-P coating demonstrated superior abrasive performance and corrosion resistance compared to Ni-W and Ni-P alloy coatings, as has been extensively discussed [12-17]. The codeposited W element enhanced the high tensile strength and thermal stability of the coating layer in the furnace. The development of ternary Ni-W-P coatings has achieved low coefficients of friction and mechanical properties to replace chromium due to environmental issues. Due to the advantages of ternary Ni-W-P coatings, such as tensile strength, thermal stability and corrosion resistance, much effort has been devoted to ternary Ni-W-P alloy deposition methodology. An amorphous Ni-W-P coating was electrodeposited on steel, and then the erosion-corrosion test was employed to investigate the eroded surface of the specimen at impact velocities of 3.14, 5.23, and 8.37 m/s [18]. As XRD, the amorphous Ni-W-P transitioned to Ni₄W and Ni₃P after the work-hardening process. Additionally, the hardness and corrosion resistance increased significantly with the impact velocity. The multilayer coating technique was executed to deposit Ni-P and ternary Ni-W-P on steel, and a heat treatment (200-600°C) was performed to strengthen the mechanical properties [19]. The presence of the Ni₃P phase beyond 400°C promoted hardness and corrosion resistance after the heat-treatment process. Ternary Ni-W-P was coated on martensitic stainless steel with deposition times of 15, 30 and 60 minutes [20]. The corrosion resistance of the coating layer increased with the deposition time in the presence of a nodular structure on the coating layer. The pulse electroplating technique was used to coat Ni-W-P alloys on copper, and the effects of temperature, pH, current density, and duty cycle were induced on the experimental parameters [21]. It was shown that the content of P and W correlated to the bath temperature, and the P-element plating declined with the current density. The coating layer effectively decreased the corrosion current of the substrate by approximately one order of magnitude in a saline environment. A superior coating was obtained to inhibit pitting corrosion while chloride ions penetrated through the void. The nodular structure appeared on the surface, while PTFE particles were embedded on the ternary Ni-W-P coating layer [22]. The grain size and defects were inversely proportional to PTFE particles within the coating layer. The hydrophobic surface decreased with the surface energy due to the aggregation of PTFE particles.

While many studies have been performed on ternary Ni-W-P coatings, the study of mechanical performance in ternary Ni-W-P coatings has not been fully explored. The corrosion resistance, hardness and microstructure dependence on bath parameters are discussed in the present study. Furthermore, the tensile strength of the ternary Ni-W-P coating layer in saline water was investigated as well. Improving

the mechanical performance and relative properties is a critical area for the development of ternary Ni-W-P coatings in the near future.

2. EXPERIMENTAL

2.1 Specimen and mechanical test

Pure 0.3 mm thick copper was machined as the tensile test specimen; its dimensions (200 mm×20 mm×0.3 mm) conformed to the ASTM E345 standard, as shown in Fig 1. The copper substrate was immersed in a 30% Vol HCl solution at ambient temperature for 2 min and then rinsed with distilled water before immersion in the ternary Ni-W-P electrodeposited bath. Furthermore, a microhardness test was performed on the coating layer with 100 g loading force for a period of 20 seconds. The Vickers microhardness was averaged at five points to identify the hardness of the specimen. Additionally, the SSRT (slow-strain-rate test) was employed to characterize the mechanical properties, such as strength, elongation rate and stress-strain curve for ternary Ni-W-P alloys on the copper matrix after pre-treatment. The SSRT was performed at a tensile strain rate of $4 \times 10^{-6} \text{ sec}^{-1}$ in atmospheric and 3.5 wt% NaCl.

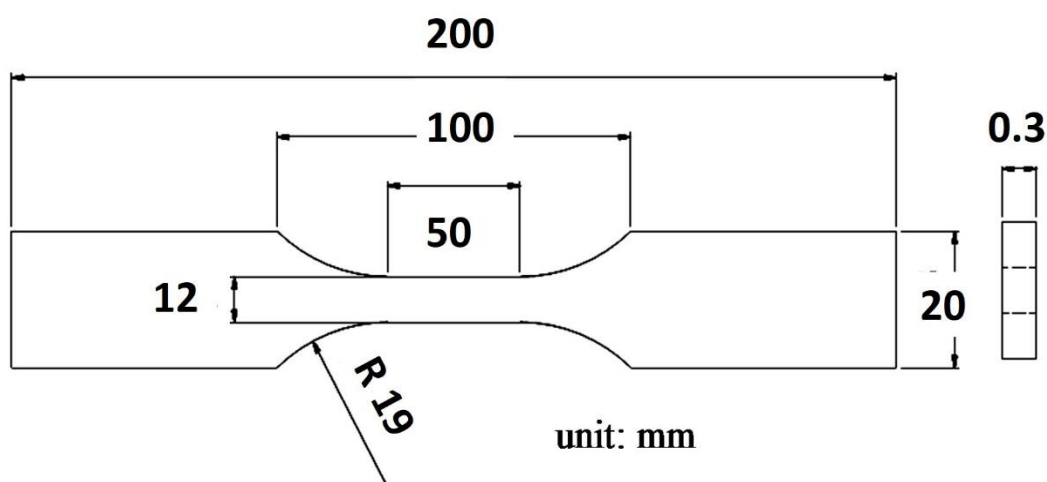


Figure 1. Tensile dimensions of the copper matrix (20 mm width by 200 mm length) for the test adhered to the ASTM-E345-standard.

2.2 Deposition system

The plating bath composition (see Table 1) was based on nickel sulfate, sodium phosphite and sodium tungstate as the main sources of Ni, P, and W, and the current densities were chosen as 1.3, 2.6, 3.9 and 5.3 A/dm². The temperature was governed at 70 °C, and the pH value was held between 5.5 and 6 with ammonia solution. To obtain the 25 μm ternary Ni-W-P alloy layer thickness, the deposition time was 120 min, as shown in Fig 2(a). The present results demonstrated perfect adhesion throughout the profile without obvious defects. A SEM (scanning electron microscope) equipped with EDAX (energy dispersive spectroscopy) was employed to investigate the composition and thickness of ternary Ni-W-P

alloys in cross-section, as shown in Fig 2(b). The EDAX was used to evaluate the composition (wt%) of Ni (82.91), W (2.96), and P (14.13) in the coating layer (1.3 A/dm² current density), as shown in Table 2. The content of P correlated with the corrosion rate of the surface, and the high content of P above 10% promoted the corrosion resistance of the coating in the present study.

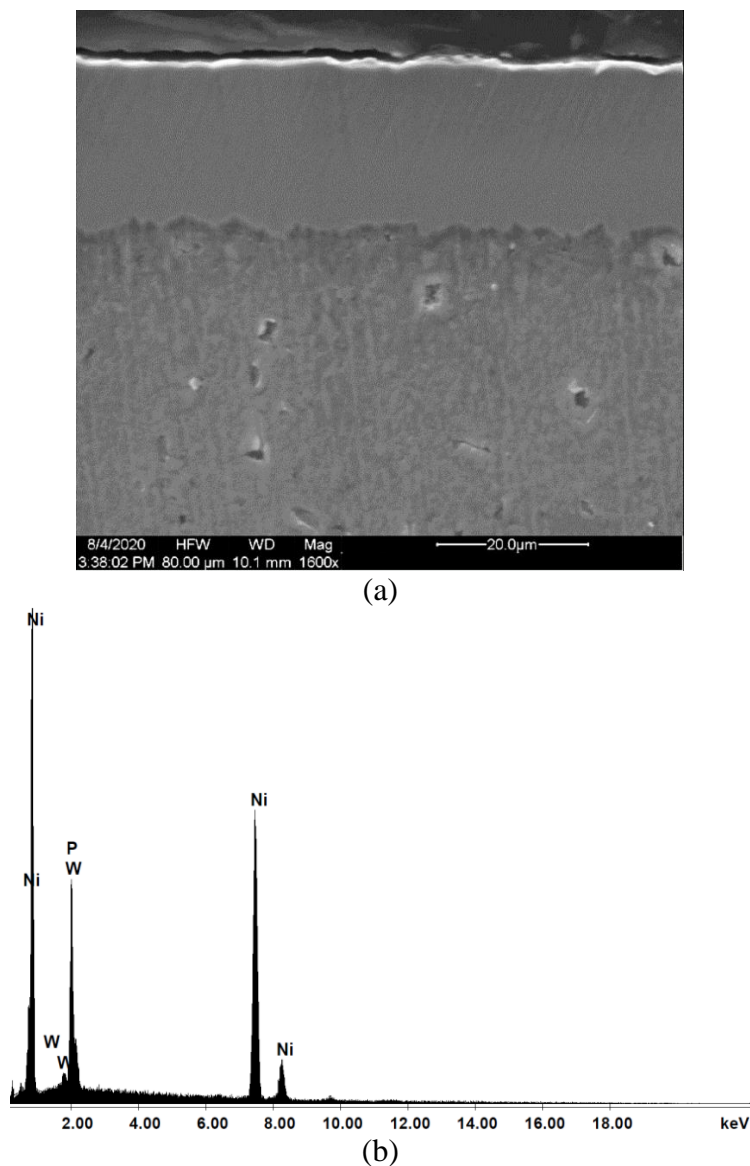


Figure 2. Investigation of the ternary Ni-W-P coating layer for specimen (current density 1.3 A/dm²): (a) Scanning Electron Microscopy (SEM) image for cross-section in thickness; (b) EDAX for the chemical composition (wt.%) were Ni (82.91), W (2.96), and P (14.13).

Table 1. Predominant constituents in the plating bath for the ternary Ni-W-P alloys.

Constituent	Quantity(Mole/L)
nickel sulfate, NiSO ₄	0.08
sodium tungstate, Na ₂ WO ₄	0.15
sodium citrate, Na ₃ C ₆ H ₅ O ₇	0.1
sodium phosphite, Na ₂ HPO ₃	0.6
citric Acid, C ₆ H ₈ O ₇	0.05

Table 2. List and chemical analysis of the ternary Ni-W-P coating between dissimilar current densities.

Current density (A/dm ²)	Element(wt%)		
	Ni	W	P
1.3	82.91	2.96	14.13
2.6	84.02	4.02	11.96
3.9	80.56	5.61	13.83
5.3	81.10	6.32	12.58

2.3 Electrochemical measurement setup

The presence of aggressive chloride ions is a major challenge for copper to exist in the oceanic environment. An electrochemical polarization cell with a three-electrode system was used to investigate the copper matrix with and without a Ni-W-P coating in a 3.5 wt% NaCl [10, 18]. Platinum served as the auxiliary electrode to supply polarizing current. An Ag/AgCl electrode and specimen were employed as the reference and working electrodes, respectively. Additionally, the potential range and scanning rate for the potentiodynamic test were -0.7 V to 0.05 V and 0.5 mV/sec, respectively. The oxidation and reduction curves intersect with the corrosion potential E_{corr} , where the charge balance between the working and auxiliary electrodes is the Tafel curve. Furthermore, the corrosion current I_{corr} was employed to evaluate the corrosion rate of the specimen, while the anodic dissolution I_a was identical to the cathodic reduction current I_c .

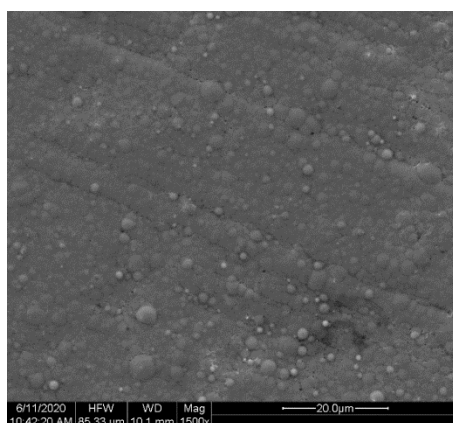
3. RESULTS AND DISCUSSION

3.1 Microstructure and hardness

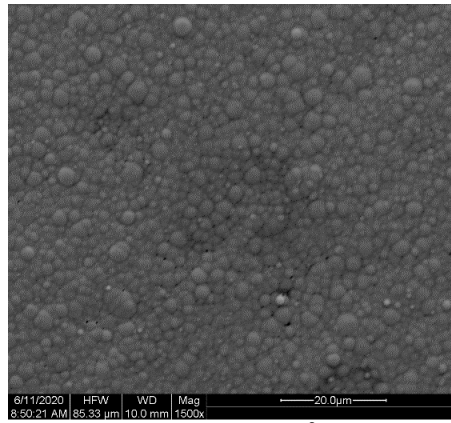
The evolution of the specimen microstructure and the amorphous phase precipitated from the basement, as shown in Fig 3. The thickness of the coating layer increased with the plating time, and the

compact morphology with 1.3 A/dm^2 current density as Fig 3(a). The spherical structure was uniformly distributed on the coating surface [14, 21]. The current density was critical to the electrodeposition process, and it dominated the kinetics of the accumulation rate for the ternary Ni-W-P coating. These secondary grains were agglomerated as main grains with some pinholes, with an average grain size of $12 \mu\text{m}$ on the morphology, and coarse grains demonstrated as columnar stacks were caused by a high current density, as shown in Fig 3(c). The current density predominated as the main driving force for the electrodeposition process, and the results indicated that the influence of the current density on the grain size varied with the reduction reaction of the tungsten element due to chemical kinetics during the plating process [22]. Apparently, the lower current density was detrimental for the precipitate of the tungsten element, as shown in Table 2. The presence of cracks, porosities and other defects was scarcely exhibited on the morphology, as shown in Fig 3, a surface micrograph of the ternary Ni-W-P coating layer. The grain grew along the column direction, and the equi-axed grain was the predominant microstructure of the ternary Ni-W-P coating.

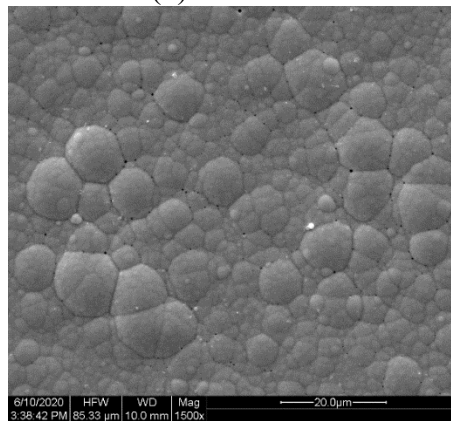
For a given current density, the roughness of the ternary Ni-W-P coating layer significantly increased with the current density, and it was investigated by AFM (atomic force microscopy), as shown in Fig 4. It was expected that the lower current density (1.3 A/dm^2) would exhibit a smooth and dense plane caused by slow kinetics of deposit on the surface. However, a bumpy surface was observed due to the rapid reduction reaction [17], while a high current density was observed in the plating bath, as shown in Fig 4(b). The line profile was investigated by AFM corresponding to the tip penetrating into the grooves. The grain size was estimated by the width of the groove; it decreased from $12 \mu\text{m}$ to $2 \mu\text{m}$ due to the current density. The maximum peak-to-valley values were approximately 1000 nm and 250 nm for current density 5.3 A/dm^2 and 1.3 A/dm^2 in the bath, respectively. On inspection of the 3D morphology as presented, the roughness corresponds well to the theoretical kinetics in chemistry, as shown in Fig 4. As expected, an increase in grain size and roughness was observed with increasing current density in the plating bath. In addition, the coarse grain structure region became larger with increasing current density in the electrodeposition process.



(a) 1.3 A/dm^2



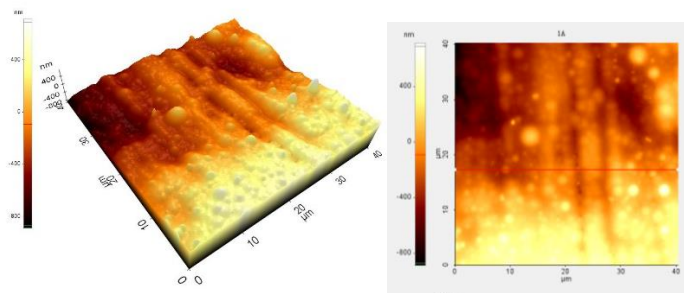
(b) 2.6 A/dm²



(c) 5.3 A/dm²

Figure 3. SEM morphology of the ternary Ni-W-P coating plated with different current densities: (a) 1.3 A/dm², (b) 2.6 A/dm², (c) 5.3 A/dm².

The experimental hardness data for the ternary Ni-W-P alloys are presented in Table 3. It was evident that the hardness increased with the current density in the plating bath, and the rapid reduction enhanced the Ni₃P phase and tungsten element to precipitate on the cathode side [16]. In comparison with Table 2, the hardness was strongly correlated with the content of tungsten, which strengthened the inherent resistance to indentation of the hardness tester [13, 19].



(a) 1.3 A/dm²

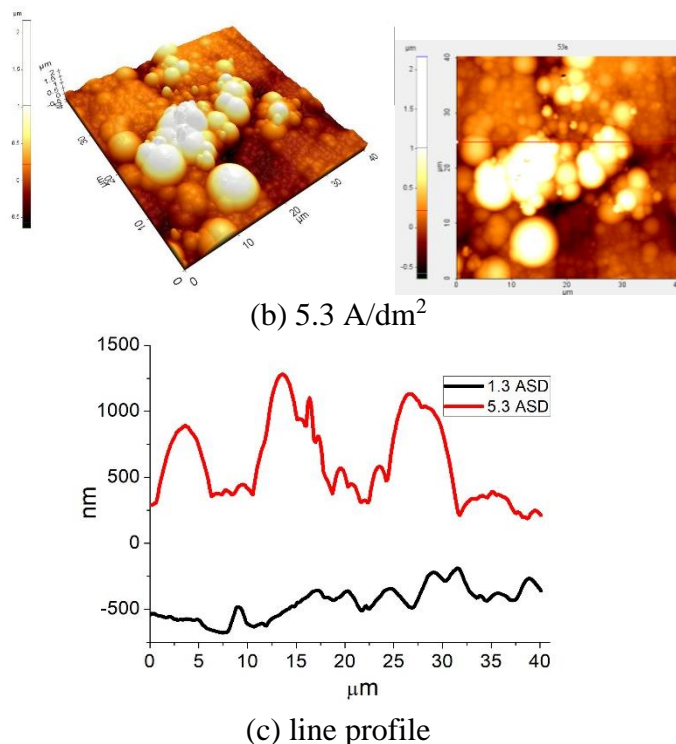


Figure 4. Topography image measured by AFM and line profile of ternary Ni-W-P alloy coatings with different current densities: (a) 1.3 A/dm², (b) 5.3 A/dm², (c) roughness profile for two AFM images.

Table 3. Hardness test of specimens.

Current density (A/dm ²)	Hardness(HV)					Mean
	1	2	3	4	5	
1.3	296.0	230.8	240.5	233.3	252.6	250.6
2.6	314.6	306.7	349.8	320.5	340.4	326.4
3.9	466.5	408.7	380.2	402.7	385.6	408.7
5.3	466.5	499.6	468.6	491.5	461.3	477.5

3.2 The electrochemistry of corrosion

The amorphous phase was characterized by superior corrosion resistance, while the volume fraction of phosphorus was heavier than 7%. The amount of the element P was 14.0% as the amorphous phase for ternary Ni-W-P alloy coatings, and it was the predominant contributor to corrosion resistance in this study. The superior corrosion resistance of the ternary Ni-W-P alloy coating provided the substrate with complete separation from the corrosive medium, and it effectively inhibited the electrochemical reaction between the coating and substrate interface. The anti-corrosion capability of the ternary Ni-W-

P alloy coatings was evaluated by measurement of its potentiodynamic polarization curve in saline water; the result is exhibited in Fig 5. The corrosion currents (I_{corr}) of the copper without and with coating (current density 1.3 A/dm²) were 5.72E⁻⁵ A/cm² and 7.01E⁻⁷ A/cm², respectively. The specimen with the protective layer significantly decreased the corrosion current density (I_{corr}) of the substrate by 2 orders of magnitude in saline water [12, 21]. It was shown that the ternary Ni-W-P alloys coated with 1.3 A/dm² current density maintained the superior anti-corrosion capability due to dense texture demonstrated on the morphology as in Fig 3(a). However, pinholes on the coating layer were caused by the rapid deposition process, and chloride ions penetrated through the pinholes from the surface to intrude on the substrate, as shown in Fig 6. The corrosion current density (I_{corr}) for high current density (5.3 A/dm²) was evidently one order of magnitude larger than that of low current density (1.3 A/dm²) due to the deposition rate in the chemical reaction. Additionally, the P content of the ternary Ni-W-P alloy coating decreased with the current density [15, 18], as shown in Table 2. The corrosion current density i_{corr} and corrosion potential E_{corr} quantify the value for the corrosion resistance of specimens as listed in Table 4.

Table 4. Corrosion characteristics of Cu substrate with and without Ni-W-P coating in 3.5 wt% NaCl by polarization measurements.

Specimen	Current density (A/dm ²)	E_{corr} (V) vs SCE	I_{corr} (A/cm ²)
Cu substrate	-	-0.26	5.72E-5
Ni-W-P alloy coating	1.3	-0.29	7.01E-7
	2.6	-0.33	8.22E-7
	3.9	-0.32	2.18E-6
	5.3	-0.36	6.22E-6

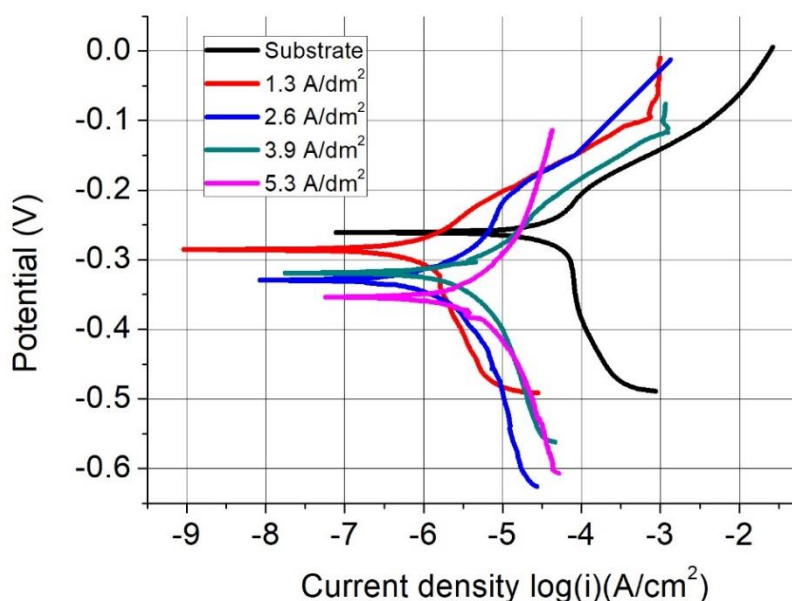


Figure 5. Potentiodynamic polarization curves (sweeping potential from -0.7 V to 0.05 V) of the ternary Ni-W-P alloy coatings in the presence of 3.5 wt% NaCl.

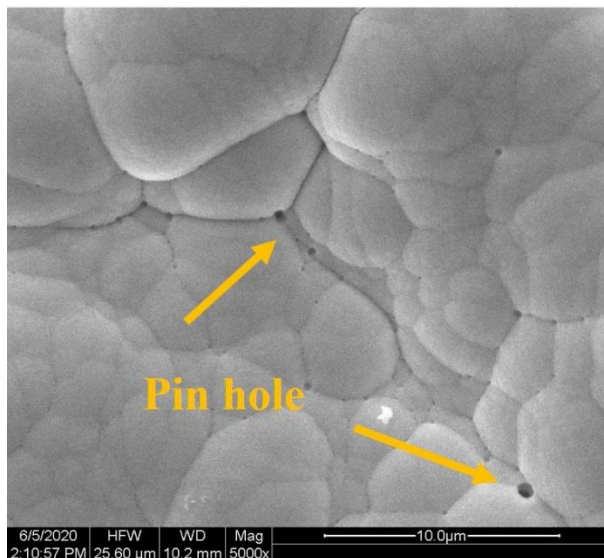


Figure 6. SEM image of pinholes on ternary Ni-W-P coating as deposited with a current density of 5.3 A/dm².

An OCP (open circuit potential) measurement was employed to record chorological potential intensity, and it was considered a criterion for the corrosion behaviour. It was evident that the substrate initially held the highest corrosion potential (-0.19 V), yet it was retained at -0.22 V at the end of immersion.

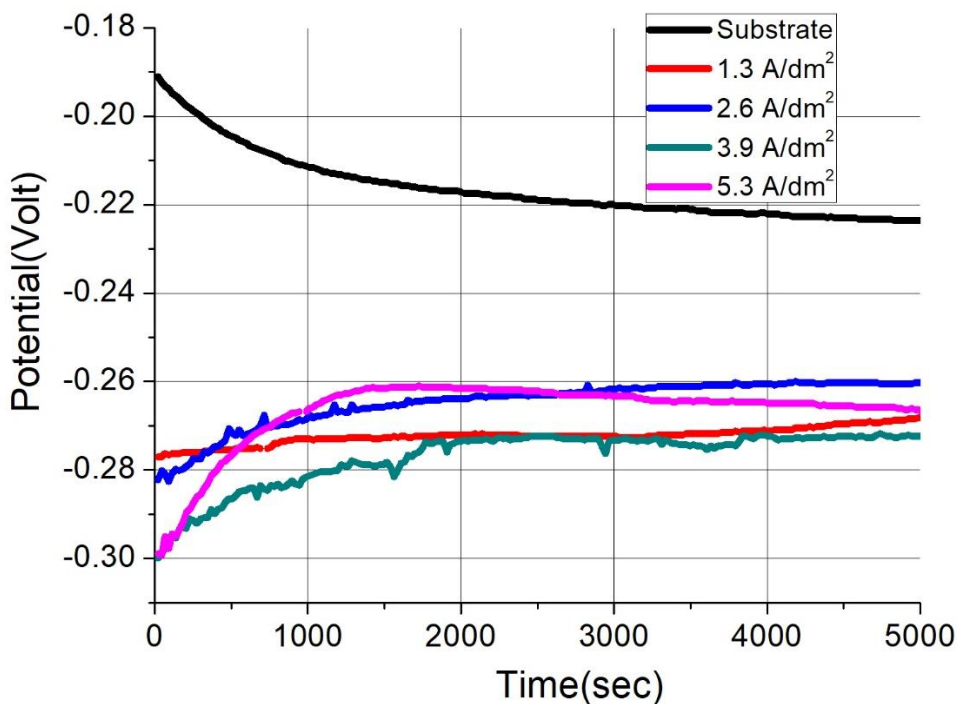
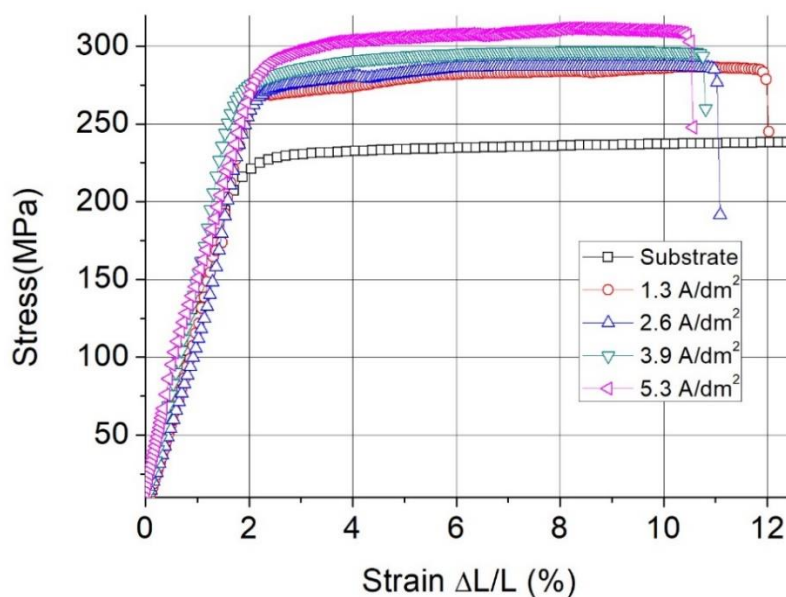


Figure 7. Time dependence on open-circuit potential of ternary Ni-W-P alloy coatings in the presence of 3.5 wt% NaCl for 5000 seconds.

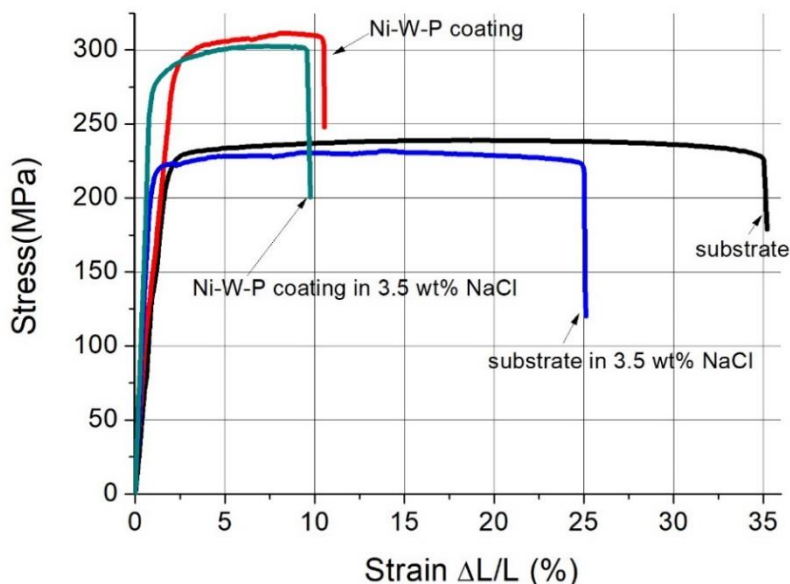
The potential of the substrate shifted significantly towards a negative value caused by anodic dissolution [10]. Conversely, a meta-stable film existed on the ternary Ni-W-P coatings as the potential shifted positively before 2000 seconds, as exhibited in Fig 7. This asymptotic potential retained with time was caused by the passive film existing on the ternary Ni-W-P alloy coating, and it approached a stable value after 2000 seconds.

3.3 Stress strain analysis

The nominal strain and tensile strength of the specimen are presented in Fig 8. The ultimate tensile strengths (UTS) of the copper matrix with and without coating were 240 and 310 MPa, respectively, and the copper matrix with coating increased by 29%. It was evident that the coating layer significantly improved the tensile resistance of the substrate, as shown in Table 5. The specimen deformed elastically behind 2% nominal strain at the initial stage, and the specimen with 5.3 A/dm² current density in the plating bath stretched up to 10.5% of strain. The tensile strengths of copper after electrodepositions with 1.3, 2.6, and 3.9 A/dm² were 283, 286 and 291 MPa, respectively. The above result demonstrated that the tensile properties of the coated specimens were determined by the current densities in the plating bath. The rise in the ultimate tensile strength was attributed to different strengthening mechanisms, such as solid solution and precipitation strengthening [23]. Moreover, the perfect adhesion of ternary Ni-W-P alloys effectively suppressed the slip band migrating to the copper surface. The strongly adhesive coating covering the substrate effectively suppressed corrosion and crack initiation behind 0.76% strain. The ternary Ni-W-P alloys suppressed the early failure of the specimen at the elastic stage, yet the chloride ion penetrated through pinholes from the surface of the coating layer towards the inner interface at the yield stage.



(a) Atmospheric environment



(b) Saline water

Figure 8. Tensile stress-strain curves (strain rate $4 \times 10^{-6} \text{ sec}^{-1}$) of copper with and without ternary Ni-W-P ternary alloy coating at 25 °C (a) in an atmospheric environment (b) in 3.5 wt% NaCl.

The results showed that the ultimate tensile strengths of the copper matrix with and without Ni-W-P alloys coating in saline water were 302 MPa and 225 MPa, respectively. Hence, the ultimate tensile strength and elongation of the substrate seriously deteriorated in the corrosive environment, as shown in Fig 8(b). The tensile stress dramatically deteriorated mechanics, such as transversal crack nucleation and propagation at the plastic deformation stage in a saline environment.

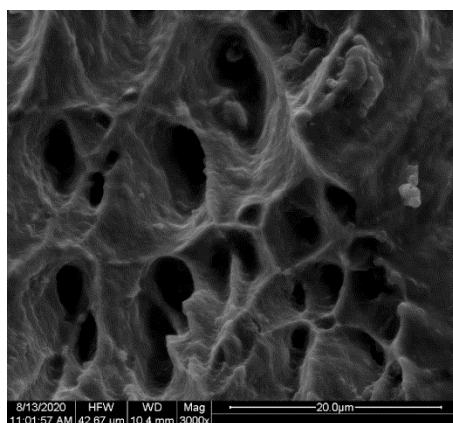
The destruction of the passive film was caused by the aqueous environment and uniaxial tensile stress with a strain rate of $4 \times 10^{-6} \text{ sec}^{-1}$. The dissolution of the anodic area was caused by the potential difference between the extrusion region and the oxide film when exposed to saline water. In the electrochemical field, the anodic reaction was that the metal dissolved while electrons were liberated from the specimen and migrated to the aqueous solution. It was concluded that the crack tip fully developed at the tip of a stress concentration and promoted the anodic dissolution of the specimen. The crack continues to propagate perpendicularly to the stress axis at the plastic deformation stage until fracture.

Table 5. Slow-strain-rate test results of copper with and without ternary Ni-W-P alloy coating at a strain rate of $4 \times 10^{-6} \text{ sec}^{-1}$ in an atmospheric environment.

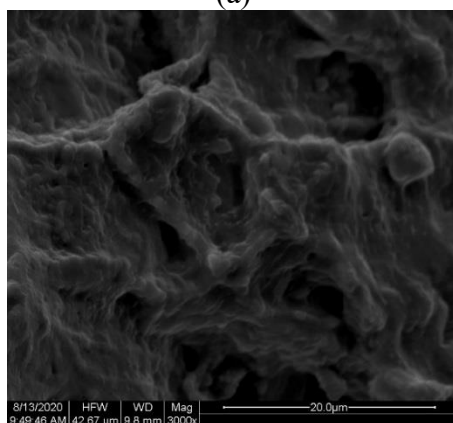
Specimen	Current density (A/dm ²)	Tensile strength (MPa)	Strain (%)
Cu substrate	-	240	35.3
Ni-W-P alloy coating	1.3	283	12.2
	2.6	286	11.3
	3.9	297	10.8
	5.3	310	10.5

3.4 Fracture Surface

These precipitations randomly distributed in voids were the main source of crack initiation. These dimples were exposed on the fracture surface, while ductile behaviour occurred with plastic flow for copper in an atmospheric environment, as shown in Fig 9(a). The damage mechanism experienced the coalescence of voids and microcrack nucleation with the crack tip, and cracks grew and propagated perpendicularly to its load direction until ductile rupture. The discrepancy between the displacements of the tensile specimen depended on the effect of the coating layer on inhibiting the propagation rate of microcracks. Hence, there was less plastic flow of the ternary Ni-W-P coating prior to microcrack propagation to the substrate. The ternary Ni-W-P coating effectively resisted the strength after deformation and promoted dislocations to accumulate on the interface between the coating layer and substrate [23]. There were fewer dimples on the ruptured surface, and the partial brittle fracture modes with coating coverage are demonstrated as cleavage fractures in Fig 9(b). Furthermore, the SEM result of acicular oxide compound on the fracture surface provided evidence that the adhesive bond within the coating layer was seriously deteriorated while the SSRT executed in 3.5 wt% NaCl as Fig 9(c). The above experiment concluded that the physical mechanism involved cohesive failure to fracture when the specimen was exposed in an aqueous environment.



(a)



(b)

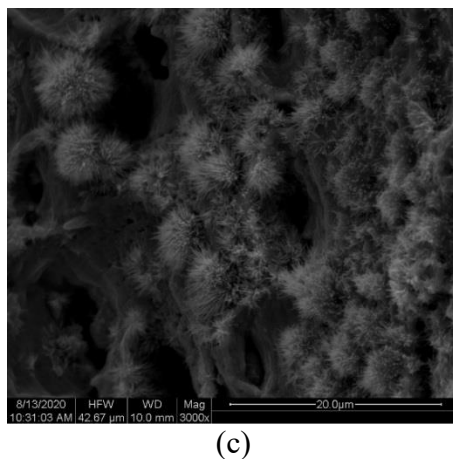


Figure 9. SEM fractographs of copper with and without Ni-W-P coating (strain rate $4 \times 10^{-6} \text{ sec}^{-1}$): (a) substrate, (b) ternary Ni-W-P coating failure in air, and (c) ternary Ni-W-P coating failure in a saline environment.

4. CONCLUSION

A stable coating layer is critical to extensively deploy copper in oceanic environments. This paper attempts to characterize a coated ternary Ni-W-P layer on a copper matrix in corrosion and SSRT tests. First, a ternary Ni-W-P coating was electrodeposited in DC current mode with 1.3, 2.6, 3.9, and 5.3 A/dm², and it exhibited dense and crack-free morphology with fewer defects. The ternary Ni-W-P coating fabricated in the deposit system exhibited a globular structure on the surface morphology at 70 °C and a pH value between 5.5 and 6. Superior corrosion resistance was obtained at a current density of 1.3 A/dm² due to the slow electrochemical kinetics, and it exhibited smooth and defect-free morphology. The corrosion currents (I_{corr}) of the copper without and with coating (current density 1.3 A/dm²) were $5.72\text{E}^{-5} \text{ A/cm}^2$ and $7.01\text{E}^{-7} \text{ A/cm}^2$, respectively. The specimen with the protective layer significantly decreased the corrosion current density (I_{corr}) of the substrate by 2 orders of magnitude in saline water. Furthermore, the tensile strength of the specimen ranged from 283 to 310 MPa and increased with the current density (1.3 to 5.3 A/dm²); this was caused by the W content embedded in the coating layer.

At the rupture surface, there were more dimples demonstrated on the substrate, and the ductile modes with copper were demonstrated as giant plastic fractures while the SSRT was executed in an atmospheric environment. Additionally, the SSRT result also showed that a ternary Ni-W-P alloy coating was sufficient to inhibit crack initiation for the substrate in saline water. The acicular oxide compound on the fracture surface provided evidence that the adhesive bond within the coating layer was seriously deteriorated while the SSRT was executed in 3.5 wt% NaCl.

Therefore, the P and W elements co-deposited in the coating layer were the predominant corrosion and tensile resistance in this study, respectively. The composition of the deposited ternary Ni-W-P alloys was controlled by adjusting the current density of the electrodeposition process. The objectives of this work were to devise an alternative method to enhance the corrosion and tensile resistance of the copper matrix.

References

1. A. Molina, A. Torres-Islas, S. Serna, M. Acosta-Flores, R.A. Rodriguez-Diaz, J. Colin, *Int. J. Electrochem. Sci.*, 10 (2015) 1728.
2. C. H. Lin, S.Y. Tsai, *Appl. Energy*, 100 (2012) 87.
3. H.T. Wang, J.R. Wang, M.D. Ger, K.H. Hou, *Int. J. Electrochem. Sci.*, 11 (2013) 2419.
4. A. Farzaneh, M.G. Hosseini, S.K. Asl, O. Mermer, *Int. J. Electrochem. Sci.*, 11 (2016) 5140.
5. C.H. Lin, J.R. Lee, P.J. Teng, S.Y. Tsai, H.H. Sheu, K.H. Hou, M.D. Ger, *Int. J. Electrochem. Sci.*, 13 (2018) 3147.
6. S.A. Kaluzhina, O.A. Kozaderov, Y.I. Marygina, I.V. Protasova, *Int. J. Corros. Scale Inhib.*, 9 (2020) 334.
7. X.Y. Liu, Z. Xiang, J.C. Niu, K.D. Xia, Y. Yang, B.A. Yan, W. Lu, *Int. J. Electrochem. Sci.*, 10 (2015) 9042.
8. M.H. Allahyarzadeh, M. Aliofkhaezai, A.R. Rezvanian, V. Torabinejad, A.R. Sabour Rouhaghdam, *Surf. Coat. Technol.*, 307 (2016) 978.
9. Y.H. Yang, S. Liu, J.G. Li, X.F. Bian, Z.L. Guo, *Surf. Coat. Technol.*, 315 (2017) 484.
10. J. Zhang, Z.W. Song, G.Yu, B.N. Hu, X.Y. Zhang, *Int. J. Electrochem. Sci.*, 11 (2016) 10053.
11. J.L. Lv, Z.Q. Wang, T.X. Liang, S. Ken, H. Miura, *Surf. Coat. Technol.*, 337 (2018) 516.
12. Q. Zhou, W.C. Sun, M. Zhu, M.F. Tan, *Adv. Mater. Res.*, 79 (2009) 997.
13. H. Liu, R.X. Guo, Y. Zong, B.Q. He, Z. Liu, *Trans. Nonferrous Met. Soc. China*, 20 (2010) 1024.
14. S. Ranganatha, T.V. Venkatesha, K. Vathsala, *Ind. Eng. Chem. Res.*, 51 (2012) 7932.
15. H.B. Lee, M.Y. Wu, *Metall. Mater. Trans. A*, 48 (2017) 4667.
16. Q.W. Niu, Z.L. Li, G. Cui, G.D. Liu, B.Y. Wang, *Int. J. Electrochem. Sci.*, 12 (2017) 5723.
17. H. Luo, M. Leitch, H.B. Zeng, J.L. Luo, *Mater. Today Phys.*, 4 (2018) 36.
18. X.L. Ji, J.H. Zhao, S.Z. Yang, L. Gu, *Corrosion*, 69(2013) 593.
19. O.R. Oloyede, Z. Liu, M. Islam, H. Liu, R.X. Guo, *Adv. Mater. Res.*, 856 (2014) 103.
20. A. Nikitasari, E. Mabruri, *AIP conf. Proc.*, 725 (2016) 020053.
21. H.H. Zhou, Z.W. Liao, C.X. Fang, H.X. Li, B. Feng, S. Xu, G.F. Cao, Y.F. Kuang, *Trans. Nonferrous Met. Soc. China*, 28 (2018) 88.
22. L. Ren, Y.H. Cheng, Q.Q. Wang, J.Y. Yang, *Surf. Topogr. Metrol. Prop.*, 7 (2019) 045009.
23. H. Bouaziz, O. Brinza, N. Haddar, M. Gasperini, M. Feki, *Mater. Charact.*, 103 (2017) 106.